A Comparison of Nonlinear Water Wave Models

Kurt M. Berger

Department of Mathematics

The Ohio State University

231 W. 18th Ave

Columbus, OH 43210

Greg R. Baker

Department of Mathematics

The Ohio State University

231 W. 18th Ave

Columbus, OH 43210

Joel T. Johnson

Department of Electrical Engineering and ElectroScience Laboratory

The Ohio State University

205 Dreese Laboratories

2015 Neil Ave

Columbus, OH 43210

(614) 292-1593

johnson@ee.eng.ohio-state.edu

ABSTRACT

We compare the numerical evolution of one-dimensional gravity waves in response to a traveling surface pressure pulse using a highly accurate boundary integral method and two relatively efficient approximate models (West et al and Benney–Luke). In both water of finite-depth and in the deep-water limit the steady state effect of the decaying pressure ramp is to create a profile which approximates a Stokes wave. Moreover, the transient surface profile appears to evolve through a series of Stokes waves of time varying amplitude. Results show all three models to yield similar predictions for lower amplitude waves, while the West et al and boundary integral predictions differ from the Benney–Luke model at higher amplitudes.

Keywords: Water waves, boundary integral method, numerical hydrodynamics

1 Introduction

Despite significant advances in high performance computing, the direct numerical simulation of water waves remains impractical. The alternative is to develop simplified approximate models that still capture the important nonlinear aspects of water waves. Here we consider two such models (West et al and Benney–Luke) which seem to offer great promise in that they accurately capture wave-wave interactions and are also amenable to numerical solution by spectral methods. To make such models truly useful, however, we must investigate the range of wave amplitudes for which these models are reliable. In this paper, we compare results from a direct numerical simulation of one-dimensional gravity waves in response to a traveling surface pressure pulse to results from the two approximate models to investigate their ranges of validity.

The evolution of gravity waves on an inviscid, irrotational, and incompressible fluid of depth H is described by the velocity potential $\phi(x, y, z, t)$ and free surface displacement $\eta(x, y, t)$ and is governed by Laplace's equation and three boundary conditions:

$$\phi_{xx} + \phi_{yy} + \phi_{zz} = 0 \quad z < H + \eta \tag{1}$$

$$\phi_z = 0 \quad z = 0 \tag{2}$$

$$\eta_t + \eta_x \phi_x + \eta_y \phi_y - \phi_z = 0 \quad z = H + \eta \tag{3}$$

$$\phi_t + \frac{1}{2}(\nabla\phi)^2 + \frac{1}{2}\phi_z^2 + g\eta = 0 \quad z = H + \eta \tag{4}$$

Alternatively, these equations can be written in dimensionless form by choosing $g = H = 1$ or, more formally, by introducing scales for each variable. In the deep-water limit, the origin of the vertical axis is shifted to the undisturbed fluid level and the bottom boundary condition becomes $|\nabla\phi| \to 0, z \to -\infty$. In this study, we consider both the finite-depth and deep-water cases, but restrict our attention to the one-dimensional version of these equations, ignoring all terms involving the y spatial coordinate.

While analytically intractable, solutions to these equations can be found numerically using a boundary integral (vortex sheet) technique (Baker et al, 1982). In this method, the velocity potential ϕ is expressed as an integral of a dipole distribution of strength μ along the free surface, thus satisfying Laplace's equation. The potential generated by the dipole distribution must match the potential at the surface. Thus, using the surface coordinate p and surface profile $\bar{\eta}(p)$, we must have at any time t

$$\phi(p) = \frac{\mu(p)}{2} + \int \mu(q) \frac{\partial G}{\partial n(q)} \left(\bar{\eta}(p), \bar{\eta}(q)\right) dS(q) \tag{5}$$

in which $\frac{\partial G}{\partial n}$ is the normal derivative of the Laplace equation Green's function G taken with respect to the integration variable, and the integral is taken as a principal-value. For deep-water, the Green's function that of free-space; for water of finite-depth, an image surface contribution is added to ensure no vertical flow at $z = 0$.

Given initial values of $\phi(p)$ and $\bar{\eta}(p)$, Equation (5) can be solved for μ; the vector-potential can then be computed as

$$A(p) = \int \mu(q) n(p) \times \nabla G \left(\bar{\eta}(p), \bar{\eta}(q)\right) dS(q) \tag{6}$$

With the restriction to a one-dimensional surface, the vector potential reduces to an expression for the streamfunction. By differentiating both the potential and the vector-potential, the velocity at the interface is determined and the free surface $\bar{\eta}$ can be updated. Finally, ϕ is updated using the dynamic boundary equation (Equation (4)) at the surface. The computational complexity of the current implementation is $O(N^2)$, where N is the number of grid points sampling the surface profile, due to use of an iterative algorithm for solving Equation (5). The parametric representation of the surface in terms of p results in a grid spacing which is not necessarily uniform horizontally; the grid density typically increases in profile regions with more rapid spatial variations.

If the ratio of amplitude to depth is assumed to be small, an asymptotic expansion about the undisturbed fluid level allows the two surface boundary conditions to be reduced to a single equation for the velocity potential, from which the surface profile η can be found. The expansion is expressed in terms of parameter $\epsilon = \frac{a}{H} << 1$, in which a is the scale for the surface profile η. Benney and Luke (1964) derived such an equation for waves in shallow water, although this type of expansion

was used earlier by Hasselmann (1961) to describe wave-wave interactions. Recently, Milewski and Keller (1998) derived a similar evolution equation for water of finite-depth; the extension to deep-water is straightforward. The one-dimensional, finite-depth version of the Benney–Luke equation, in which $O(\epsilon^3)$ terms are ignored, is given as follows:

$$u_{tt} + \mathcal{L}u + \epsilon\mathcal{N}_1(u,u) + \epsilon^2\mathcal{N}_2(u,u,u) = 0 \tag{7}$$

with quadratic terms

$$\mathcal{N}_1(u,u) = 2u_x u_{xt} + 2\mathcal{L}u\mathcal{L}u_t + u_t u_{xx} - u_t\mathcal{L}u_{tt} \tag{8}$$

and cubic terms

$$\begin{aligned}\mathcal{N}_2(u,u,u) &= u_t\mathcal{L}u_t(u_{xx} - \mathcal{L}^2u) + 2u_t(u_{xxt}\mathcal{L}u - u_{xt}\mathcal{L}u_x - u_x\mathcal{L}u_{xt}) \\ &\quad + \frac{1}{2}u_{xx}\left(3u_x^2 - (\mathcal{L}u)^2\right) + \frac{1}{2}\mathcal{L}^2u\left(u_x^2 + (\mathcal{L}u)^2\right) + 2u_x\mathcal{L}u\mathcal{L}u_x\end{aligned} \tag{9}$$

In this dimensionless equation $u(x,t) = \phi(x,1,t)$ is the velocity potential at the undisturbed free surface and $\mathcal{L}$ is the pseudo-differential operator $\mathcal{L} = (-\partial_{xx})^{\frac{1}{2}}\tanh\left[(-\partial_{xx})^{\frac{1}{2}}\right]$. The water surface is given by $1 + \epsilon\eta(x,t)$, where

$$\eta = -u_t + \epsilon\mathcal{T}_1(u,u) + \epsilon^2\mathcal{T}_2(u,u,u) + ... \tag{10}$$

with

$$\mathcal{T}_1(u,u) = u_t\mathcal{L}u_t - \frac{1}{2}\left(u_x^2 + (\mathcal{L}u)^2\right) \tag{11}$$

and

$$\mathcal{T}_2(u,u,u) = u_t(u_x\mathcal{L}u_x - u_{xx}\mathcal{L}u + \frac{1}{2}u_t u_{xxt}) - u_t(\mathcal{L}u_t)^2 + \frac{1}{2}\mathcal{L}u_t\left(u_x^2 + (\mathcal{L}u)^2\right) \tag{12}$$

The same equations apply for gravity waves in deep-water except that $\mathcal{L} = (-\partial_{xx})^{\frac{1}{2}}$. Equation (7) can not be integrated numerically in the form given because of the quadratic term $-u_t\mathcal{L}u_{tt}$ in the $\mathcal{N}_1$ term . If we replace u_{tt} with $-\mathcal{L}u - \epsilon\mathcal{N}_1(u,u) + O(\epsilon^2)$ in this term, we obtain $u_t\mathcal{L}^2u$ in the equation

for $\mathcal{N}_1(u,u)$, and we must add the additional cubic term $u_t\mathcal{L}[\mathcal{N}_1(u,u)]$ to $\mathcal{N}_2$. Because all nonlinear terms in this formulation can be calculated pseudospectrally, the computational complexity of the solution is $O(N\log N)$ when a uniform grid is employed. In principle, the expansion can be continued beyond the $O(\epsilon^3)$ terms described above, but the required analytic derivation of the expressions becomes very tedious.

Another major approach to analyzing the water wave equations, due to Zakharov (for example, Zakharov 1999), is to rewrite the two free-surface boundary conditions in terms of the velocity potential at the surface $\phi^s(x,y,t)$ and note that the resulting equations are derivable from a single Hamiltonian. By expanding this Hamiltonian in orders of η, Zakharov has derived the coefficients governing wave interactions for both the finite-depth and deep-water regimes. Following the Zakharov approach, West et al (1987) use an expansion of ϕ^s in orders of η and an expansion of ϕ_z about the undisturbed fluid level to derive an efficient algorithm for the evolution of η and the velocity potential at the surface. Defining the velocity potential at the surface as $\phi^s(x,t)=\phi(x,\eta(x,t),t)$ and letting $W(x,t)=\phi_z(x,\eta(x,t),t)$, the surface boundary conditions may be rewritten as follows:

$$\eta_t = -\eta_x\phi^s_x + W(1+\eta_x^2) \tag{13}$$

$$\phi^s_t = -g\eta - \frac{1}{2}(\phi^s_x)^2 + \frac{1}{2}W^2(1+\eta_x^2) \tag{14}$$

The unique aspect of the West et al method lies in the computation of W, which is difficult since ϕ is known only at the surface. By expanding ϕ^s in orders of η and also expanding ϕ_z about the undisturbed fluid level, W can be expressed as a series in terms of pseudo-spectral products of η and ϕ_s. The expansion is easily automated to allow calculation of arbitrary order contributions, and the algorithm is $O(N\log N)$ when a uniform grid is employed. The "high order spectral method" (Dommermuth and Yue, 1987) for hydrodynamic evolution of a surface is an equivalent hydrodynamic technique based on a similar expansion. In the results to be illustrated, terms up to 6th order in η were included. However, as discussed in (West et al, 1987), the higher–order products of η and ϕ_s encountered in computing W result in an oversampling requirement in order to retain a specified spectral content for the profile; this requirement will be shown to influence the number of surface profile grid points needed in the comparison between methods.

2 Simulation parameters

In our experiments, the generation of waves is initiated by a traveling surface pressure pulse of decaying amplitude with the form:

$$P(x,t) = a(t)e^{i(k_o x - \omega_o t)} + * \tag{15}$$

where $*$ refers to the complex conjugate and the complex amplitude is given by

$$a(t) = \alpha \frac{A}{\omega_0^2} e^{-\alpha t^2}(2\alpha t^2 - 1 + 2i\omega_o t) \tag{16}$$

This form of the pressure was chosen so that a traveling wave of wavenumber k_o, frequency ω_o, and steady state amplitude A is a solution to the linearized water wave equations. Here α controls the rate of decay of the pressure as well as the time to reach the steady state wave height. When the above pressure-forcing term is included on the left-hand-side of the dynamic boundary condition, each of the three water wave models must be modified accordingly. This modification is straightforward in the Vortex and West et al methods as the pressure term enters the equations directly. For Benney–Luke, the addition of the pressure term P results in the forcing term

$$-P_t(k_o x - \omega_o t) + \epsilon\left(P_t \mathcal{L} u_t - P_x u_x - P(u_{xx} + \mathcal{L}^2 u)\right) \tag{17}$$

on the right-hand side of Equation (7).

In all of our experiments we pick a spatial domain, assumed periodic, of length $L = 2\pi$. The initial condition is an undisturbed fluid surface $\eta(x,0) = 0$, $\phi(x,z,0) = 0$. Our choice for the pressure parameters are $\alpha = \frac{1}{(400)^2}$, $A = 0.3$, $k_o = 1$ and $\omega_o^2 = |k_o|\tanh(|k_o|)$ for finite-depth and $\omega_o^2 = |k_o|$ for deep-water. This choice of A should produce a final profile for which nonlinear effects are observable, while the value of α used will ensure that temporal variations in the pressure ramp occur over the scale of several wave periods in the linear dynamics case (i.e. the Gaussian function multiplying the pressure reaches e^{-1} at T=400, while the linear wave period is less than 8 time units.)

The Benney–Luke model is evolved in time using a 4th-order Runge-Kutta scheme ($\Delta t = 0.01$) while the West et al and boundary integral models use a 4th-order predictor–corrector scheme

($\Delta t = 0.01$). These choices of time step values are sufficient so that the amplitudes presented are accurate within approximately 10^{-6} for all the times considered. The number of gridpoints for each method is chosen such that the change in the amplitudes a_1, a_2, and a_3 is less than 10^{-6} when the number of gridpoints is doubled. For the West et al method, $N_x = 64$ gridpoints were used for both the deep-water and finite-depth cases, while $N_x = 32$ points were used in the Benney–Luke and boundary integral methods for all experiments. The higher sampling rate required for the West et al method is a consequence of the higher order products inherent in the method, as discussed previously.

3 Results

Figures 1 and 2 plot the temporal evolution of the first four modes of a cosine transform of the surface profile for the deep-water and finite-depth cases, respectively. Curves are included for all three methods up to a final time of $T = 1200$; results from the boundary integral code are interpolated to a regular grid to allow simple computation of the cosine transform. In both the deep-water and finite-depth cases, increasing mode amplitudes are observed for times less than 400, while relaxation to lower steady state amplitudes follows at later times. Note the steady state amplitude obtained for mode one is significantly less than the linear value of 0.3, indicating that non-linear interactions are playing an important role in the temporal evolution. Good general agreement is observed among the three methods for all cases, with the West et al and boundary integral code amplitudes remaining within 0.1% for all times and all amplitudes considered. These small differences make the boundary integral and West et al results indistinguishable in the plots illustrated. Larger differences between the West et al and boundary integral methods are observed for higher mode numbers, but these amplitudes are sufficiently small to make comparisons susceptible to other errors. The Benney-Luke method shows a somewhat larger error for modes one through four, particularly at larger mode amplitudes and for the fourth mode in the deep-water case. These errors are due to the lower order used in the Benney-Luke code implemented (third-order versus sixth-order terms in the West et al results). Moreover, the calculation of η in Equation (10) for

the Benney–Luke is also only third-order. Adding more terms to this latter expansion is relatively easy, but is meaningless unless higher-order terms are included in the Benney–Luke equation itself. This is a daunting task (and a limitation of the method) as the number of terms at each successive order grows very rapidly.

Since the mode amplitudes plotted in Figures 1 and 2 converge to a steady state, comparison with Stokes' wave solutions is considered in Figures 3 and 4 for the deep-water and finite-depth cases, respectively. The time evolution of mode $|a_2|$ versus $|a_1|$ and mode $|a_3|$ versus $|a_1|$ every $t = 1$ for each method is plotted in these figures, as well as a similar comparison for the exact Stokes' wave over the given range of amplitudes. Note that the density of data points in these graphs is lowest near the origin where the pressure function is increasing most rapidly. The exact Stokes' wave is computed using a method outlined by Schwartz (1974) for water at any depth, and checked with the method of Longuet-Higgins (1985) for water of infinite depth. Results show the boundary integral and West et al methods to track the exact Stokes' wave curve well as the pressure function changes even through the increasing, relaxation, and steady state portions of the time evolution. The Benney-Luke curve shows some deviations, again primarily at higher amplitudes.

4 Conclusion

The results of this study show the West et al method to provide highly accurate computations for Stokes waves up to ka_1 products of approximately 0.18 in deep water and 0.13 in finite depth (the maximum values obtained in response to the traveling pressure pulse considered.) The Benney-Luke approach also provides generally accurate computations, but shows some errors particularly in the finite depth case and in the fourth and higher modes for deep water. The particular simulation considered demonstrates the formation of an approximately "adiabatically evolving" Stokes wave in response to a slowly varying traveling pressure pulse.

References

[1] Baker, G. R., D. Meiron, and S. Orszag (1982) Generalized vortex methods for free surface flow problems, *J. Fluid Mech.,* **123**, 477–501.

[2] Benney, D. J. and J.C. Luke (1964) Interactions of permanent waves of finite amplitude, *J. Math. Phys.,* **43**, 309-313.

[3] Dommermuth, D. G. and D. K. P. Yue (1987) A high-order spectral method for the study of non-linear gravity waves, *J. Fluid Mech.,* **184**, 267–288.

[4] Hasselmann, K. (1961) On the nonlinear energy transfer in gravity-wave spectra: part I, general theory, *J. Fluid Mech.,* **12**, 481–500.

[5] Longuet-Higgins, M. S. (1985) Bifurcation in gravity waves, *J. Fluid Mech.,* **151**, 457-475.

[6] Milewski, P. and J. Keller (1998) Three-dimensional water waves, *Stud. Appl. Math.* **37**, 149.

[7] Schwartz, L. W. (1974) Computer extension and analytic continuation of Stokes' expansion for gravity waves, *J. Fluid Mech.,* **62**, 553-578.

[8] West, B. J., K. Brueckner, R. Janda, D. Milder, and R. Milton (1987) A new numerical method for surface hydrodynamics, *J. Geophys. Res.,* **92**, 11803-11824.

[9] Zakharov, V. (1999) Statistical theory of gravity and capillary waves on the surface of a finite-depth fluid, *Eur. J. Mech. B / Fluids,* **18**, 327-344.

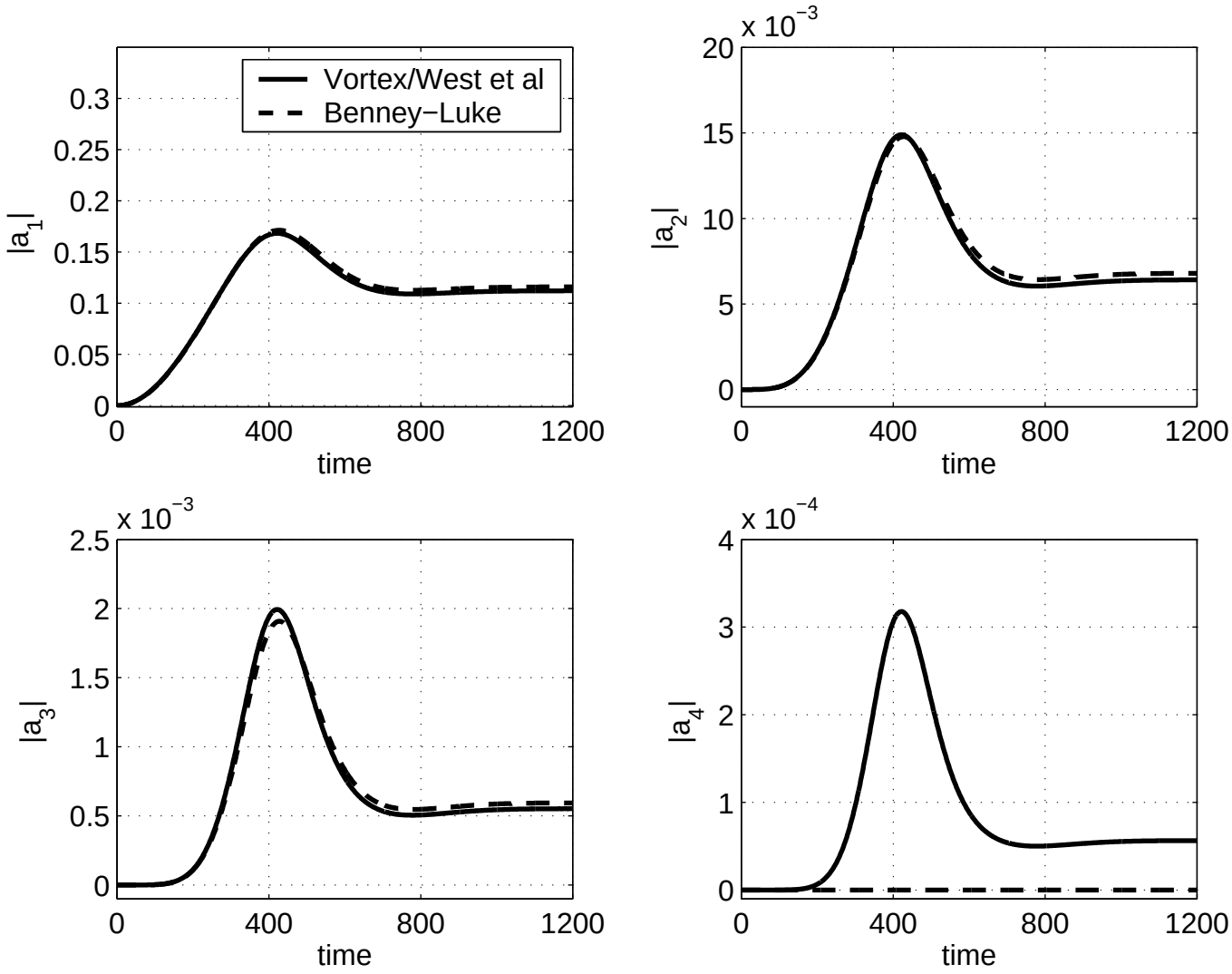

Figure 1: Evolution of modes $|a_1|$, $|a_2|$, $|a_3|$, and $|a_4|$ for the *deep–water* case. Vortex and West et al results are indistinguishable in the plots shown.

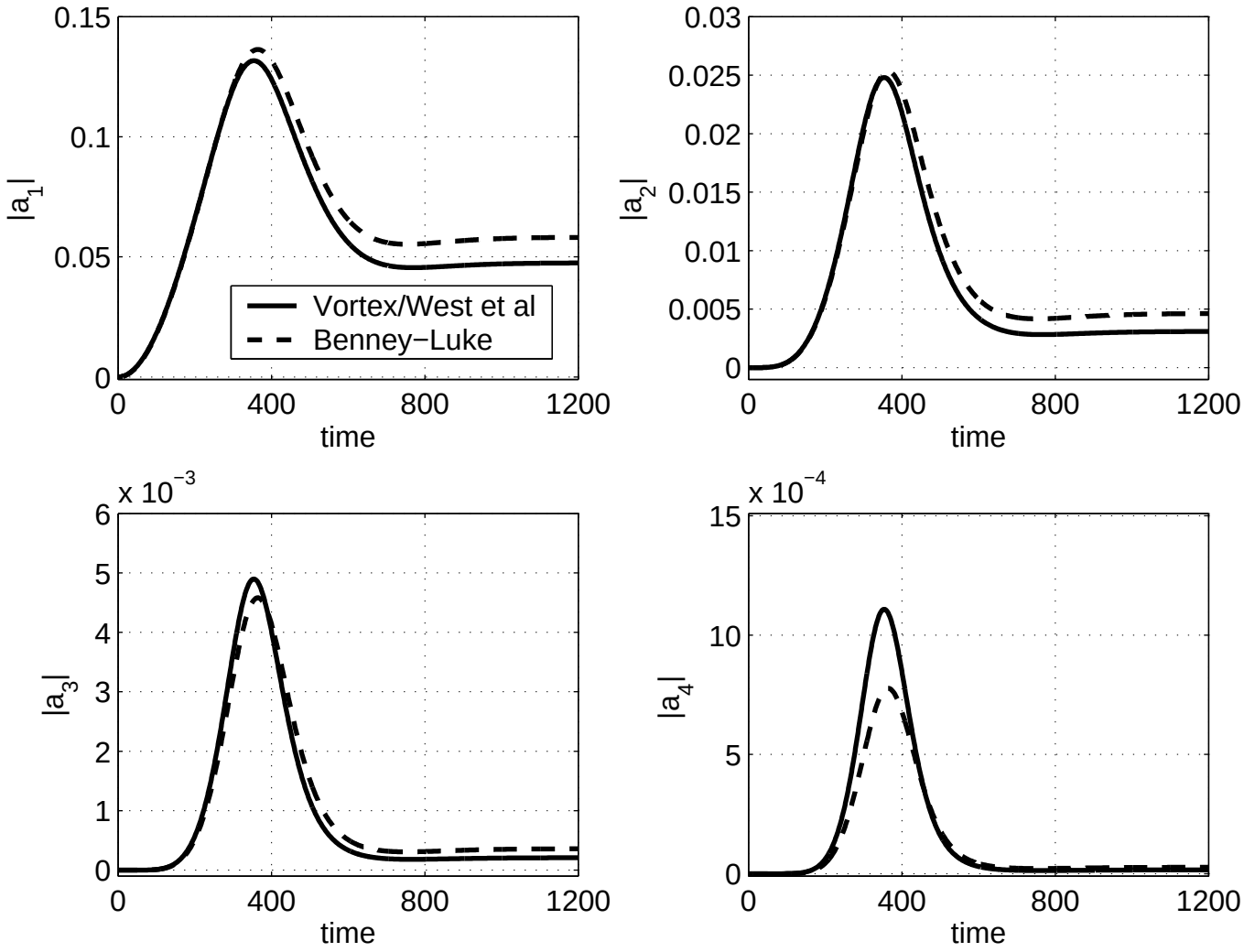

Figure 2: Evolution of modes $|a_1|$, $|a_2|$, $|a_3|$, and $|a_4|$ for the *finite-depth* case. Vortex and West et al results are indistinguishable in the plots shown.

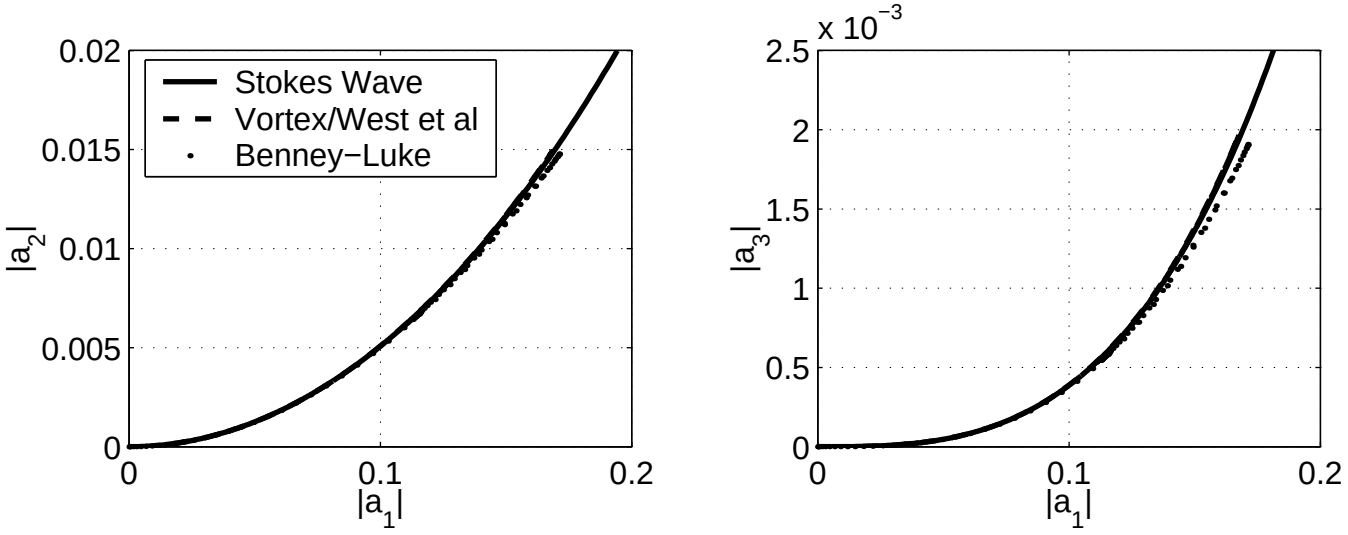

Figure 3: Evolution of modes $|a_2|$ versus $|a_1|$ and $|a_3|$ versus $|a_1|$ for the *deep–water* ca se. Vortex and West et al results are indistinguishable in the plots shown.

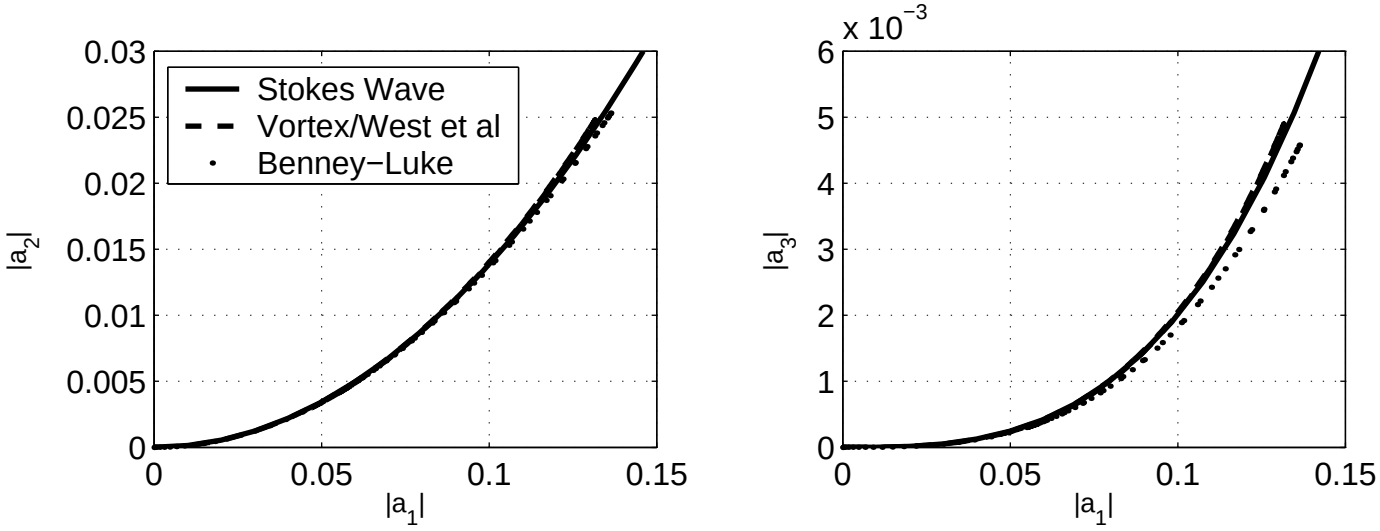

Figure 4: Evolution of modes $|a_2|$ versus $|a_1|$ and $|a_3|$ versus $|a_1|$ for the *finite-depth* case. Vortex and West et al results are indistinguishable in the plots shown.